PHOTONICS Research

# Negative refraction mediated by bound states in the continuum

Zhanyuan Zhang,[1] Feifei Qin,[1] Yi Xu,[1,2,*] Songnian Fu,[2] Yuncai Wang,[2] and Yuwen Qin[2]

[1]Department of Electronic Engineering, College of Information Science and Technology, Jinan University, Guangzhou 510632, China
[2]Advanced Institute of Photonics Technology, School of Information Engineering, and Guangdong Provincial Key Laboratory of Information Photonics Technology, Guangdong University of Technology, Guangzhou 510006, China
*Corresponding author: yi.xu@osamember.org

Received 7 April 2021; revised 2 June 2021; accepted 6 June 2021; posted 7 June 2021 (Doc. ID 427094); published 30 July 2021

**Negative refraction might occur at the interface between a two-dimensional photonic crystal (PhC) slab and a homogeneous medium, where the guiding of the electromagnetic wave along the third dimension is governed by total internal reflection. Herein, we report on the observation of negative refraction in the PhC slab where the vertical guiding is enabled by a bound state in the continuum and essentially beyond the light cone. Such abnormal refraction and guiding mechanism are based on the synchronous crafting of spatial dispersion and the radiative lifetime of Bloch modes within the radiative continuum. Microwave experiments are provided to further validate the numerical proposal in an all-dielectric PhC platform. It is envisioned that the negative refraction observed beyond the light cone might facilitate the development of optical devices in integrated optics, such as couplers, multiplexers, and demultiplexers.** 

https://doi.org/10.1364/PRJ.427094

## 1. INTRODUCTION

Envisioned by Veselago in the 1960s [1], abnormal refraction has received intense research efforts from the photonics community with long-term quests for new possibility and functionality [2–18], including but not limited to comprehensive manipulation of spacetime wave packets [2,14], generalized laws of reflection and refraction [12], negative refraction [4–6,10,11,15], superprism [8,9], self-collimation [13,14], and optical lensing [15]. In particular, the two-dimensional negative refraction in a photonic crystal (PhC) slab provides on-chip solutions for molding the flow of light in an unparalleled manner [5,7–11,13,14,17]. To date, the guiding mechanism of light along the slab normal for such on-chip negative refraction strictly relies on the effect of total internal reflection, which inevitably imposes a fundamental limitation that such negative refraction can only be achieved below the light cone of surrounding medium.

Bound state in the continuum (BIC) possessing nontrivial physical properties resembles a new physical mechanism to localize a wave within the radiative continuum [19]. Optical BIC, an analogue of their quantum counterpart [20], provides an effective way to guide light beyond total internal reflection [21–27]. Especially, the BIC of the PhC slab becomes a versatile platform for exploring new physics and applications in integrated photonic systems [28–63]. Optical guiding becomes possible when the radiative loss of guiding modes is compatible with or smaller than the loss originated from the intrinsic material absorption and fabrication associated disorder effects [14,42,55,57,58].

In this paper, we investigate numerically and demonstrate experimentally the negative refraction in all-dielectric PhC slabs, where the guiding along the slab normal is enabled by quasi-BICs as schematically shown in Fig. 1(a). The radiative lifetime and spatial dispersion of leaky modes in the PhC slab are manipulated simultaneously to enable the observation of negative refraction mediated by quasi-BICs. Microwave experiments are provided to further support our numerical proposal.

## 2. PRINCIPLE

The PhC slab used to realize negative refraction mediated by BIC is shown in Fig. 1(a), which consists of dielectric pillars arranged in a triangle lattice. The unit cell of the PhC slab is shown in Fig. 1(b). The principle of negative refraction beyond the light cone is schematically presented in Fig. 1(c), where spatial dispersion and $Q$ factors of modes in the PhC slab are tailored in the radiative continuum simultaneously. In contrast to conventional negative refraction guided by total internal reflection, the radius of equi-frequency contour (EFC) for the negative refraction modes (red dashed circle) is smaller than the radius of the EFC for the light cone (blue dashed circle) at the same frequency as shown in Fig. 1(c). At the same time, if such modes can be tuned to become quasi-BICs, negative refraction can be achieved without relying on total internal reflection. In this case, an incident plane wave from air with

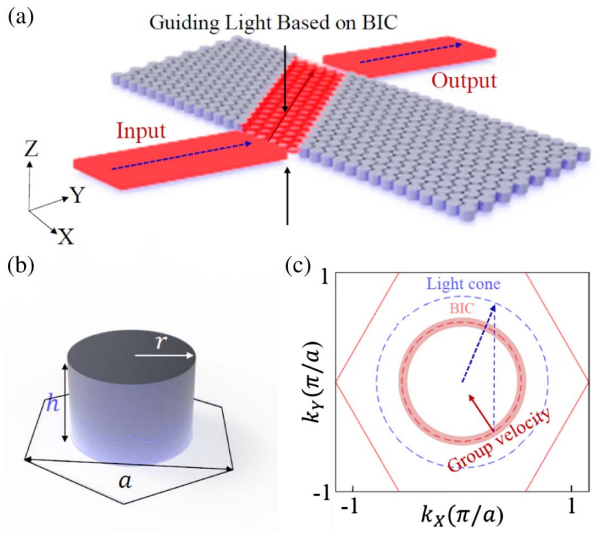


**Fig. 1.** (a) Schematic of negative refraction mediated by bound state in the continuum (BIC), where the vertical guiding is based on the BIC. A Gaussian beam is used to excite negative refraction modes as indicated by arrows. (b) A unit cell of the PhC slab is formed by a dielectric pillar (relative permittivity $\varepsilon_r = 11.56$, $r = 0.4819a$) arranged in a triangular lattice with the lattice constant $a$, and its height $h$ is $0.6627a$. (c) Physical mechanism enabling the negative refraction beyond the light cone of the surrounding materials. The red dashed circle indicates the equi-frequency contour (EFC) for the negative refraction modes above the light cone, where the associated BIC and quasi-BIC regions are outlined by the red shadow ring. The blue dashed circle represents the EFC of light cone at the same frequency. The blue dashed arrow indicates the $k$-vector of the incident plane wave from air, while the red arrow corresponds to the group velocity of the Bloch mode excited in the PhC slab. The solid red line shows the boundary of the first Brillouin zone (FBZ). The vertical blue dashed line indicates the preservation of momentum parallel to the interface during refraction.

a $k$-vector indicated by the blue dashed arrow will excite a mode of the PhC slab whose direction of group velocity outlined by the red arrow is at the same side of the interface normal as schematically shown in Fig. 1(c). The magnitude of the $k$-vector for the excited Bloch mode is smaller than the incident one. As a result, such mode is within the radiative continuum, where the vertical guiding is enabled by the quasi-BICs as indicated by the red ring shape high-$Q$ regions overlapped with the EFC in momentum space.

The dispersion relationship of the considered band (Γ-M) and the corresponding $Q$ factors for the all-dielectric PhC slab shown in Fig. 1(b) are presented in Figs. 2(a) and 2(b). Such modal dispersions are calculated by the finite element method (FEM), where the eigenvalues of the source-free Maxwell equation are evaluated. Bloch boundary conditions are applied to the hexagonal boundary outlined in Fig. 1(b), while perfectly matched layers are used perpendicularly to the $\pm Z$ directions. The height $h$ of the dielectric rod is $0.6627a$, where $a$ is the lattice constant outlined in Fig. 1(b) while the ratio $r/a$ is indicated in the insets of Figs. 2(a) and 2(b). The relative permittivity of the dielectric pillars is $\varepsilon_r = 11.56$, and we neglect the absorption loss first. As can be seen from Fig. 2(a), the slope of the band ($\partial\omega/\partial k$) is negative, indicating the morphology of EFC manifests as shrinking circles toward the Γ-point when the frequency is increased [4], as shown by the black solid lines in Fig. 2(c). This kind of mode can be used to realize negative refraction at the interface between the PhC slab and air. For example, an incident plane wave with the $k$-vector indicated by the blue dashed arrow will excite the Bloch mode of the PhC, exhibiting negative refraction whose propagation direction is at the same side of the interface normal as the incident one. Because of the momentum conservation parallel to the interface, the $k$-vector of the excited Bloch mode can be determined by matching the tangential $k$-vector of the excited Bloch mode. As a result, the propagation direction of the refracted Bloch wave [$v = \nabla_k \omega(k)$, red solid arrow] is normal to the EFC, which is determined by the continuity condition of the tangential components of the wavevector, as indicated by the blue dashed line, through momentum conservation [4]. However, these modes are located within the radiative continuum, which means that they are leaky in general. As can be seen from Fig. 2(b), there is a symmetry protected BIC (at-Γ point) and accidental BICs (off-Γ point) supported by the PhC slab. As the off-Γ BIC is not protected by the

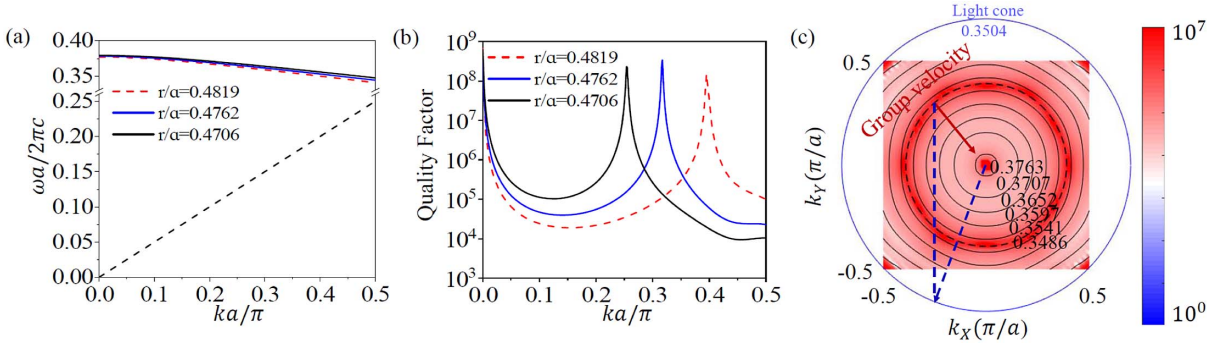


**Fig. 2.** (a) Dispersion properties of PhC slab along the Γ-M direction for three different lattice constants, where the $r/a$ is indicated in the legend. The light cone (black dashed line) is also presented. (b) The corresponding $Q$ factors for the modes shown in (a). (c) The calculated EFCs and the corresponding $Q$ factors of a square region within the first Brillouin zone. The light cone ($a/\lambda = 0.3504$) is indicated by the blue solid circle. The EFCs for different modes at the same band are marked in the figure, while the color code represents the corresponding $Q$ factors. The blue dashed arrow shows the $k$-vector of the incident plane wave from air, while the red solid arrow corresponds to the group velocity of the mode excited in the PhC slab. The vertical dashed line indicates the preservation of momentum during refraction.

symmetry incompatibility between the continuum and the BIC mode [19], the positions of the off-Γ BIC in momentum space can be effectively tuned by varying the parameter $r/a$ [Fig. 2(b)], while the dispersion of such band is hardly affected [Fig. 2(a)]. Therefore, Bloch modes with the characteristic of negative refraction dispersion can be manipulated to become quasi-BICs simultaneously by adjusting the $r/a$, which facilitates the realization of the negative refraction beyond the light cone. As can be seen from Fig. 2(c), the morphology of locations for the quasi-BIC modes ($Q > 10^7$, color coded) in the momentum space resembles the shape of the EFC (black dashed circle). Such synchronous manipulation of spatial dispersion and radiative lifetime of Bloch modes enables the realization of negative refraction beyond the light cone.

In order to evaluate the negative refraction, we calculate the propagation of a Gaussian beam with a polarization of $H_z$ through a finite PhC slab by the FEM. The Gaussian beam is used to excite the quasi-TE mode of the PhC slab where the dominant magnetic field is normal to the slab. Perfectly matched layer boundary conditions are used to absorb the outgoing wave. The size of the finite PhC slab considered is about $\sim 41 \times 19\, a^2$, which would introduce an effective Fabry–Perot cavity along the propagation direction because of the abrupt variation of the permittivity. The distributions of magnetic field [Re($H_z$)] on the central $x$–$y$ plane under the excitation of a Gaussian beam with different tiled angles ($\theta_1 = 10°$ and $\theta_2 = 20°$) are shown in Figs. 3(a) and 3(b). As indicated in these figures, the refracted beams in the PhC slab are at the same side of the interface normal as the input beams, and the phase fronts of the incident and outgoing beams are parallel to each other. In order to validate that such negative refraction is indeed beyond the light cone, which is enabled by the quasi-BICs rather than total internal reflection, the effective $k$-vectors of the refracted beam in the PhC slab are evaluated along the refraction directions indicated by the red arrows in PhC slab, where a Fourier transform of the complex magnetic field ($H_z$) along a line at the center of the beam is performed. Both results are approximately equal to $0.192\,\pi/a$ for Figs. 3(a) and 3(b), respectively, which are smaller than the $k$-vector of the incident one. Therefore, these modes are essentially beyond the light cone, where the out-of-plane scattering can be dramatically reduced by quasi-BICs.

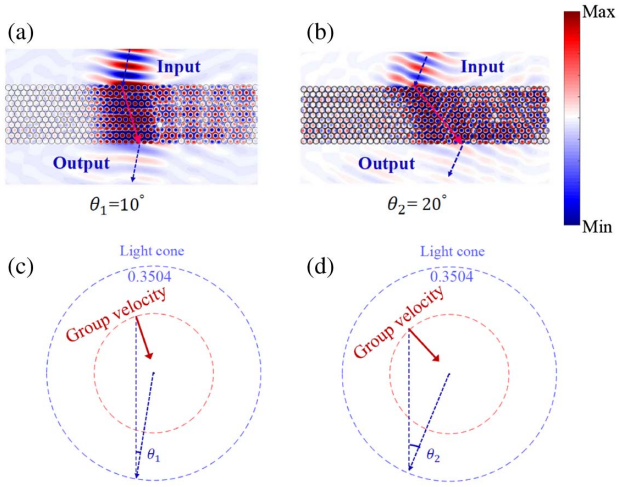


**Fig. 3.** (a) and (b) Evolution of the magnetic field [Re($H_z$)] on the central $x$–$y$ plane when a Gaussian beam ($a/\lambda = 0.3504$) is incident into the PhC slab with two different incident angles ($\theta_1 = 10°$ and $\theta_2 = 20°$). The directions of the incident, refracted, and outgoing waves are indicated by blue dashed, red solid, and blue dashed arrows, respectively. (c) and (d) EFC analysis of negative refraction for the results shown in (a) and (b), respectively. The blue dashed and red solid arrows indicate the $k$-vector of the incident wave and the group velocity of the wave refracted by the PhC slab. The red dashed circles represent the EFC of negative refraction modes, whose out-of-plane scattering is prohibited by the quasi-BICs. The blue dashed circles represent their corresponding light cones at the same frequency, respectively.

We further provide the EFC-based interpretations of negative refraction in Figs. 3(c) and 3(d). The EFC supporting negative refraction at the normalized frequency $a/\lambda = 0.3504$ is shown by the red dashed circle, while the EFC of light cone (air) at the same frequency is also shown by the blue dashed circle. As can be seen from these figures, different incident angles will result in negative refraction with different refraction angles. The negative propagation angles extracted from Figs. 3(a) and 3(b) coinciding with that are obtained from the EFC analysis shown in Figs. 3(c) and 3(d). The coupling efficiency to the negative refraction modes can be optimized by engineering the morphology of the interfaces or using waveguide couplers [9].

## 3. MICROWAVE EXPERIMENTS

The physical mechanism of negative refraction mediated by quasi-BIC is general, and it can be applied over a wide spectral range of electromagnetic waves. Here we experimentally demonstrate the negative refraction phenomenon in microwaves. The experimental setup for near-field measurement of magnetic field and the PhC slab fabricated by alumina ceramics are shown in Fig. 4(a). A standard-gain horn antenna (HD-58SGAH20N) is connected to a vector network analyzer (VNA, R&S ZNB40), which is used to generate an electromagnetic wave packet (5 to 7 GHz) with a polarization of $E_x$ and mimic the scenario of Gaussian beam excitation. The width of the horn antenna is approximately 4 times the electromagnetic wave's wavelength. Furthermore, in order to flatten the wavefront of excited field, the horn antenna is more than 10 working wavelengths away from the PhC slab. A homemade loop antenna, whose acquired $S_{21}$ is proportional to the magnetic field $H_z$, is mounted on a scanning platform (LINBOU, NFS03 Floor Version) connected to the VNA. Microwave absorbers are used to minimize the impact of echo signals. The dashed red rectangle indicates the scan area above the PhC slab, where the acquired Re($S_{21}$) map can be used to qualitatively inspect the distribution of magnetic field. The PhC slab used in the experiment is composed of alumina disks ($\varepsilon_r = 9.6$, $r = 8$ mm, $h = 11$ mm) arranged in a triangle lattice ($a = 17$ mm) that is placed on a foam substrate ($\varepsilon_r \sim 1$).

The EFCs (black solid lines) and corresponding $Q$ factors (color coded) of the alumina PhC slab used in the experiment are shown in Fig. 4(b). Similar negative refraction can be achieved compared with the results in Fig. 2, though a different relative permittivity of PhC slab is used. Similarly, the $k$-vector

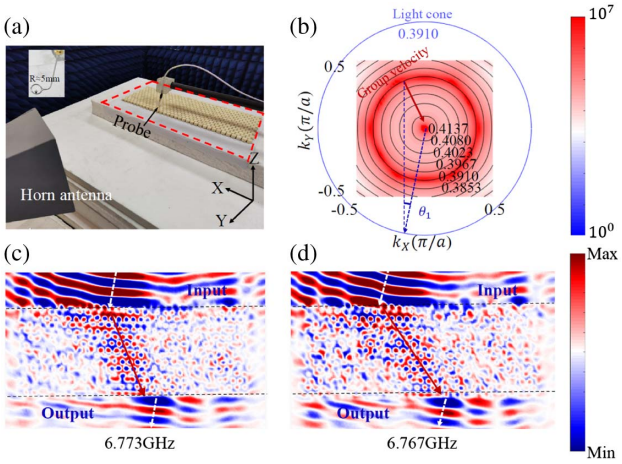


**Fig. 4.** (a) Experimental setup and the fabricated dielectric PhC slab used to demonstrate the negative refraction mediated by quasi-BICs. The red dashed rectangle indicates the measured area in the experiment. (b) The calculated EFCs (black solid lines) and the corresponding $Q$ factors (color coded) of a square region within the FBZ for the PhC slab used in experiment. The blue circle indicates the EFC of light cone ($a/\lambda = 0.391$). (c) and (d) Experimental results of near-field mapping of Re($S_{21}$) of a loop antenna at frequencies of 6.773 GHz and 6.767 GHz for incident angles of 10° and 15°, respectively. The parallel dashed lines indicate the boundaries of the PhC slab.

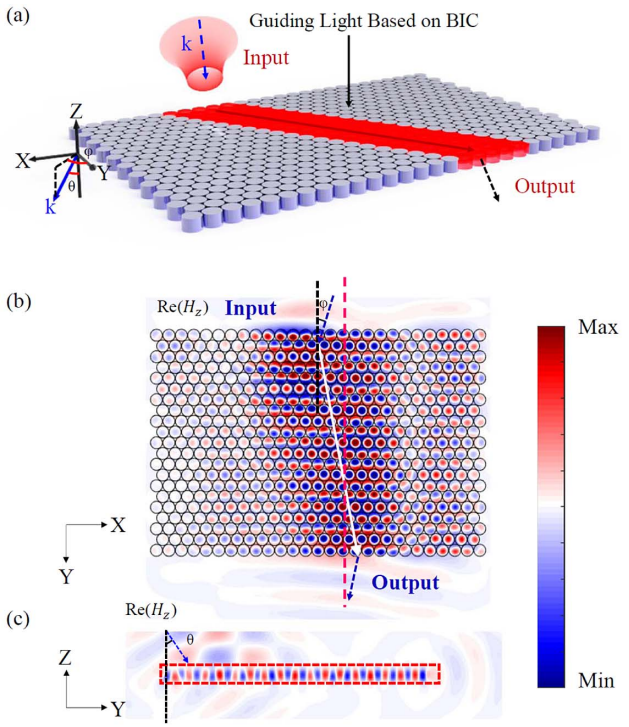


**Fig. 5.** Coupling of a Gaussian beam with a stereo incident angle to the on-chip negative refraction mode mediated by the quasi-BICs. The angle between the incident $k$-vector and the $y$ ($z$) axis is $\varphi = 15°$ ($\theta = 30°$). The structure is similar to that in Fig. 3. Distributions of the calculated magnetic field [Re($H_z$)] on the central (b) $x$–$y$ plane and (c) $y$–$z$ plane at the red dashed line shown in (b) are presented. The red dashed square indicates the location of the PhC slab.

(blue dashed line) of the incident plane wave from air and the group velocity of the refractive wave are at the same side of the surface normal. By turning the angles between the horn antenna and the $y$ direction, negative refraction with different refracted angles similar to Figs. 3(a) and 3(b) can be realized. The distributions of Re($S_{21}$) measured at the red dashed rectangle marked in Fig. 4(a) for different incident angles are shown in Figs. 4(c) and 4(d), respectively. Signatures of negative refraction at the interface between air and PhC slab are clearly observed in the experiment results as indicated by the red arrows. The directions of $k$-vectors extracted from Fig. 4(c) are similar to the analysis based on the EFC shown in Fig. 4(b), and the phase fronts of the incident and outgoing waves obtained in experiment are parallel to each other. The extracted $k$-vectors in the PhC slab for the results in Figs. 4(c) and 4(d) are $0.16672\pi/a$ and $0.16852\pi/a$, respectively, which are smaller than the incident one ($0.38382\pi/a$ and $0.38352\pi/a$). It should be pointed out that there is small discrepancy between the quasi-BICs obtained in experiment and simulation, which might be originated from the imperfection of PhC structures. These microwave results indicate that negative refraction mediated by quasi-BICs can be observed in experiment.

Furthermore, negative refraction mediated by quasi-BIC provides an unique opportunity for coupling excitations in the continuum to quasi-guiding modes exhibiting negative refraction, as schematically shown in Fig. 5(a), breaking the limitation that negative refraction can only be achieved in the two-dimensional plane for a PhC slab. In order to visualize this possibility, we calculate the coupling of an inclined (30°) Gaussian beam (relative to the two-dimensional plane) to the PhC slab at an angle of $\varphi = 15°$ with respect to the $y$ axis and $\theta = 30°$ with respect to the $z$ axis. The full width at half-maximum of the Gaussian beam is $\lambda$, where $\lambda$ is the wavelength of the Gaussian beam. The distributions of the magnetic field [Re($H_z$)] on the central $x$–$y$ and $y$–$z$ planes are shown in Figs. 5(b) and 5(c), respectively. As we can see from the figures, the stereo inclined Gaussian beam indeed excites a quasi-guiding negative refraction beam in the PhC slab, which might facilitate potential applications in integrated optics, such as optical multiplexing and optical couplers. The coupling efficiency can be improved by using unidirectional BIC [58], while the quasi-guiding properties can be enhanced by the recently proposed merging BICs at off-high symmetry points [63].

## 4. DISCUSSION AND CONCLUSION

In summary, we propose a physical mechanism to realize negative refraction beyond the light cone based on the quasi-BICs. The real and imaginary parts of the eigenfrequency for the Bloch mode, which are corresponding to spatial dispersion and radiative lifetime of the Bloch mode, are tailored simultaneously to achieve negative refraction beyond total internal reflection. The direction of negative refraction can be controlled by the direction of the incident wave. Microwave experiments are used to further validate the numerical results. The operating-frequency range of negative refraction mediated by

quasi-BICs might be enlarged by applying the mechanism of merging BICs near the accidental BIC. It is anticipated that negative refraction beyond the light cone can effectively facilitate the coupling between free space and the on-chip negative refraction modes, which could open up an avenue for exploring abnormal refraction within the radiative continuum and find applications in optical couplers, multiplexing, and mode sorting. Furthermore, it could also shed new light on the generalization of negative refraction in other wave-physics systems.

**Funding.** National Key Research and Development Program of China (2018YFB1801001); National Natural Science Foundation of China (91750110); Guangdong Introducing Innovative and Entrepreneurial Teams of the Pearl River Talent Recruitment Program (2019ZT08X340); Research and Development Plan in Key Areas of Guangdong Province (2018B010114002); Pearl River Nova Program of Guangzhou (201806010040).

**Disclosures.** The authors declare no conflicts of interest.

**Data availability.** Data underlying the results presented in this paper are not publicly available at this time but may be obtained from the authors upon reasonable request.

## REFERENCES

1. V. G. Veselago, "The electromagnetics of substances with simultaneously negative values of $\varepsilon$ and $\mu$," Sov. Phys. Usp. **10**, 509–514 (1968).
2. B. Bhaduri, M. Yessenov, and A. F. Abouraddy, "Anomalous refraction of optical spacetime wave packets," Nat. Photonics **14**, 416–421 (2020).
3. J. B. Pendry, A. J. Holden, W. J. Stewart, and I. Youngs, "Extremely low frequency plasmons in metallic mesostructures," Phys. Rev. Lett. **76**, 4773–4776 (1996).
4. M. Notomi, "Theory of light propagation in strongly modulated photonic crystals: refraction like behavior in the vicinity of the photonic band gap," Phys. Rev. B **62**, 10696–10705 (2000).
5. C. Luo, S. G. Johnson, J. D. Joannopoulos, and J. B. Pendry, "All-angle negative refraction without negative effective index," Phys. Rev. B **65**, 201104 (2002).
6. C. Luo, S. G. Johnson, and J. D. Joannopoulos, "All-angle negative refraction in a three-dimensionally periodic photonic crystal," Appl. Phys. Lett. **81**, 2352–2354 (2002).
7. T. Pertsch, T. Zentgraf, U. Peschel, A. Bräuer, and F. Lederer, "Anomalous refraction and diffraction in discrete optical systems," Phys. Rev. Lett. **88**, 093901 (2002).
8. H. Kosaka, T. Kawashima, A. Tomita, M. Notomi, T. Tamamura, T. Sato, and S. Kawakami, "Superprism phenomena in photonic crystals," Phys. Rev. B **58**, R10096 (1998).
9. L. Wu, M. Mazilu, and T. F. Krauss, "Beam steering in planar-photonic crystals: from superprism to supercollimator," J. Lightwave Technol. **21**, 561–566 (2003).
10. S. Kocaman, R. Chatterjee, N. C. Panoiu, J. F. McMillan, M. B. Yu, R. M. Osgood, D. L. Kwong, and C. W. Wong, "Observation of zeroth-order band gaps in negative-refraction photonic crystal superlattices at near-infrared frequencies," Phys. Rev. Lett. **102**, 203905 (2009).
11. H. J. Lezec, J. A. Dionne, and H. A. Atwater, "Negative refraction at visible frequencies," Science **316**, 430–432 (2007).
12. N. Yu, P. Genevet, M. A. Kats, F. Aieta, J. P. Tetienne, F. Capasso, and Z. Gaburro, "Light propagation with phase discontinuities: generalized laws of reflection and refraction," Science **334**, 333–337 (2011).
13. L. Gan, F. Qin, and Z. Y. Li, "Broadband large-angle self-collimation in two-dimensional silicon photonic crystal," Opt. Lett. **37**, 2412–2414 (2012).
14. Y. Lin, T. Feng, S. Lan, J. Liu, and Y. Xu, "On-chip diffraction-free beam guiding beyond the light cone," Phys. Rev. Appl. **13**, 064032 (2020).
15. T. Xu, A. Agrawal, M. Abashin, K. J. Chau, and H. J. Lezec, "All-angle negative refraction and active flat lensing of ultraviolet light," Nature **497**, 470–474 (2013).
16. H. E. Kondakci and A. F. Abouraddy, "Diffraction-free space–time light sheets," Nat. Photonics **11**, 733–740 (2017).
17. M. Lequime and C. Amra, "Anomalous refraction of a low divergence monochromatic light beam in a transparent slab," Opt. Lett. **43**, 1419–1422 (2018).
18. C. Liu, L. Chen, T. Wu, Y. Liu, J. Li, Y. Wang, Z. Yu, H. Ye, and L. Yu, "All-dielectric three-element transmissive Huygens'metasurface performing anomalous refraction," Photon. Res. **7**, 1501–1510 (2019).
19. C. W. Hsu, B. Zhen, A. D. Stone, J. D. Joannopoulos, and M. Soljačić, "Bound states in the continuum," Nat. Rev. Mater. **1**, 16048 (2016).
20. J. V. Neumann and E. P. Wigner, "Über merkwürdige diskrete eigenwerte," Phys. Z. **30**, 465–467 (1929).
21. D. C. Marinica, A. G. Borisov, and S. V. Shabanov, "Bound states in the continuum in photonics," Phys. Rev. Lett. **100**, 183902 (2008).
22. E. N. Bulgakov and A. F. Sadreev, "Bound states in the continuum in photonic waveguides inspired by defects," Phys. Rev. B **78**, 075105 (2008).
23. Y. Plotnik, O. Peleg, F. Dreisow, M. Heinrich, S. Nolte, A. Szameit, and M. Segev, "Experimental observation of optical bound states in the continuum," Phys. Rev. Lett. **107**, 183901 (2011).
24. S. Weimann, Y. Xu, R. Keil, A. E. Miroshnichenko, A. Tünnermann, S. Nolte, A. A. Sukhorukov, A. Szameit, and Y. S. Kivshar, "Compact surface Fano states embedded in the continuum of waveguide arrays," Phys. Rev. Lett. **111**, 240403 (2013).
25. C. L. Zou, J. M. Cui, F. W. Sun, X. Xiong, X. B. Zou, Z. F. Han, and G. C. Guo, "Guiding light through optical bound states in the continuum for ultrahigh-$Q$ microresonators," Laser Photon. Rev. **9**, 114–119 (2015).
26. Z. Hu and Y. Y. Lu, "Propagating bound states in the continuum at the surface of a photonic crystal," J. Opt. Soc. Am. B **34**, 1878–1883 (2017).
27. Z. Yu, X. Xi, J. Ma, H. K. Tsang, C.-L. Zou, and X. Sun, "Photonic integrated circuits with bound states in the continuum," Optica **6**, 1342–1348 (2019).
28. S. I. Azzam and A. V. Kildishev, "Photonic bound states in the continuum: from basics to applications," Adv. Opt. Mater. **9**, 2001469 (2021).
29. J. Lee, B. Zhen, S.-L. Chua, W. Qiu, J. D. Joannopoulos, M. Soljačić, and O. Shapira, "Observation and differentiation of unique high-$Q$ optical resonances near zero wave vector in macroscopic photonic crystal slabs," Phys. Rev. Lett. **109**, 067401 (2012).
30. C. W. Hsu, B. Zhen, J. Lee, S. L. Chua, S. G. Johnson, J. D. Joannopoulos, and M. Soljačić, "Observation of trapped light within the radiation continuum," Nature **499**, 188–191 (2013).
31. E. N. Bulgakov and D. N. Maksimov, "Light guiding above the light line in arrays of dielectric nanospheres," Opt. Lett. **41**, 3888–3891 (2016).
32. Y. Yang, C. Peng, and Z. Li, "Semi-analytical approach for guided mode resonance in high-index-contrast photonic crystal slab: TE polarization," Opt. Express **21**, 20588–20600 (2013).
33. Y. Yang, C. Peng, Y. Liang, Z. Li, and S. Noda, "Analytical perspective for bound states in the continuum in photonic crystal slabs," Phys. Rev. Lett. **113**, 037401 (2014).
34. B. Zhen, C. W. Hsu, L. Lu, A. D. Stone, and M. Soljačić, "Topological nature of optical bound states in the continuum," Phys. Rev. Lett. **113**, 257401 (2014).
35. X. Gao, C. W. Hsu, B. Zhen, X. Lin, J. D. Joannopoulos, M. Soljačić, and H. Chen, "Formation mechanism of guided resonances and bound states in the continuum in photonic crystal slabs," Sci. Rep. **6**, 31908 (2016).
36. E. N. Bulgakov and A. F. Sadreev, "Propagating Bloch bound states with orbital angular momentum above the light line in the array of dielectric spheres," J. Opt. Soc. Am. A **34**, 949–952 (2017).

37. A. Kodigala, T. Lepetit, Q. Gu, B. Bahari, Y. Fainman, and B. Kanté, "Lasing action from photonic bound states in continuum," Nature **541**, 196–199 (2017).
38. Z. F. Sadrieva, I. S. Sinev, K. L. Koshelev, A. Samusev, I. V. Iorsh, O. Takayama, R. Malureanu, A. A. Bogdanov, and A. V. Lavrinenko, "Transition from optical bound states in the continuum to leaky resonances: role of substrate and roughness," ACS Photon. **4**, 723–727 (2017).
39. A. Tittl, A. Leitis, M. Liu, F. Yesilkoy, D. Y. Choi, D. N. Neshev, Y. S. Kivshar, and H. Altug, "Imaging-based molecular barcoding with pixelated dielectric metasurfaces," Science **360**, 1105–1109 (2018).
40. S. T. Ha, Y. H. Fu, N. K. Emani, Z. Pan, R. M. Bakker, R. Paniagua-Domínguez, and A. I. Kuznetsov, "Directional lasing in resonant semiconductor nanoantenna arrays," Nat. Nanotechnol. **13**, 1042–1047 (2018).
41. K. Koshelev, S. Lepeshov, M. Liu, A. Bogdanov, and Y. Kivshar, "Asymmetric metasurfaces with high-*Q* resonances governed by bound states in the continuum," Phys. Rev. Lett. **121**, 193903 (2018).
42. S. Dai, L. Liu, D. Han, and J. Zi, "From topologically protected coherent perfect reflection to bound states in the continuum," Phys. Rev. B **98**, 081405 (2018).
43. Y. Zhang, A. Chen, W. Z. Liu, C. W. Hsu, B. Wang, F. Guan, X. H. Liu, L. Shi, L. Lu, and J. Zi, "Observation of polarization vortices in momentum space," Phys. Rev. Lett. **120**, 186103 (2018).
44. M. Minkov, I. A. D. Williamson, M. Xiao, and S. Fan, "Zero-index bound states in the continuum," Phys. Rev. Lett. **121**, 263901 (2018).
45. Y. He, G. T. Guo, T. H. Feng, Y. Xu, and A. E. Miroshnichenko, "Toroidal dipole bound states in the continuum," Phys. Rev. B **98**, 161112 (2018).
46. H. M. Doeleman, F. Monticone, W. den Hollander, A. Alù, and A. F. Koenderink, "Experimental observation of a polarization vortex at an optical bound state in the continuum," Nat. Photonics **12**, 397–401 (2018).
47. S. I. Azzam, V. M. Shalaev, A. Boltasseva, and A. V. Kildishev, "Formation of bound states in the continuum in hybrid plasmonic-photonic systems," Phys. Rev. Lett. **121**, 253901 (2018).
48. M. Liu and D.-Y. Choi, "Extreme Huygens' metasurfaces based on quasi-bound states in the continuum," Nano Lett. **18**, 8062–8069 (2018).
49. F. Yesilkoy, E. R. Arvelo, Y. Jahani, M. Liu, A. Tittl, V. Cevher, Y. Kivshar, and H. Altug, "Ultrasensitive hyperspectral imaging and biodetection enabled by dielectric metasurfaces," Nat. Photonics **13**, 390–396 (2019).
50. G. Zito, S. Romano, S. Cabrini, G. Calafiore, A. C. D. Luca, E. Penzo, and V. Mocella, "Observation of spin-polarized directive coupling of light at bound states in the continuum," Optica **6**, 1305–1312 (2019).
51. Z. Sadrieva, K. Frizyuk, M. Petrov, Y. Kivshar, and A. Bogdanov, "Multipolar origin of bound states in the continuum," Phys. Rev. B **100**, 115303 (2019).
52. W. Liu, B. Wang, Y. Zhang, J. Wang, M. Zhao, F. Guan, X. Liu, L. Shi, and J. Zi, "Circularly polarized states spawning from bound states in the continuum," Phys. Rev. Lett. **123**, 116104 (2019).
53. A. S. Kupriianov, Y. Xu, A. Sayanskiy, V. Dmitriev, Y. S. Kivshar, and V. R. Tuz, "Metasurface engineering through bound states in the continuum," Phys. Rev. Appl. **12**, 014024 (2019).
54. W. Chen, Y. Chen, and W. Liu, "Singularities and poincaré indices of electromagnetic multipoles," Phys. Rev. Lett. **122**, 153907 (2019).
55. Z. Liu, Y. Xu, Y. Lin, J. Xiang, T. Feng, Q. Cao, J. Li, S. Lan, and J. Liu, "High-*Q* quasibound states in the continuum for nonlinear metasurfaces," Phys. Rev. Lett. **123**, 253901 (2019).
56. F. Wu, J. Wu, Z. Guo, H. Jiang, Y. Sun, Y. Li, J. Ren, and H. Chen, "Giant enhancement of the Goos-Hänchen shift assisted by quasibound states in the continuum," Phys. Rev. Appl. **12**, 014028 (2019).
57. J. Jin, X. Yin, L. Ni, M. Soljačić, B. Zhen, and C. Peng, "Topologically enabled ultra-high-*Q* guided resonances robust to out-of-plane scattering," Nature **574**, 501–594 (2019).
58. X. Yin, J. Jin, M. Soljačić, C. Peng, and B. Zhen, "Observation of unidirectional bound states in the continuum enabled by topological defects," Nature **580**, 467–471 (2020).
59. C. Huang, C. Zhang, S. Xiao, Y. Wang, Y. Fan, Y. Liu, N. Zhang, G. Qu, H. Ji, and J. Han, "Ultrafast control of vortex microlasers," Science **367**, 1018–1021 (2020).
60. Q. Song, J. Hu, S. Dai, C. Zheng, D. Han, J. Zi, Z. Q. Zhang, and C. T. Chan, "Coexistence of a new type of bound state in the continuum and a lasing threshold mode induced by PT symmetry," Sci. Adv. **6**, eabc1160 (2020).
61. S. Romano, M. Mangini, E. Penzo, S. Cabrini, A. C. D. Luca, I. Rendina, V. Mocella, and G. Zito, "Ultrasensitive surface refractive index imaging based on quasi-bound states in the continuum," ACS Nano **14**, 15417–15427 (2020).
62. S. Sun, Y. Ding, H. Li, P. Hu, C. W. Cheng, Y. Sang, F. Cao, Y. Hu, A. Alù, D. Liu, Z. Wang, S. Gwo, D. Han, and J. Shi, "Tunable plasmonic bound states in the continuum in the visible range," Phys. Rev. B **103**, 045416 (2021).
63. M. Kang, S. Zhang, M. Xiao, and H. Xu, "Merging bound states in the continuum at off-high symmetry points," Phys. Rev. Lett. **126**, 117402 (2021).